Computers and Concrete, *Vol. 20, No. 1 (2017) 1-10*
DOI: https://doi.org/10.12989/cac.2017.20.1.001

A tensile criterion to minimize FE mesh-dependency in concrete beams under blast loading

HanGul Gang and Hyo-Gyoung Kwak*

Department of Civil Engineering, Korean Advanced Institute of Science and Technology,
291 Daehak-ro, Yuseong-gu, Daejeon 34141, Republic of Korea

(Received November 23, 2016, Revised March 3, 2017, Accepted May 18, 2017)

Abstract. This paper focuses on the mesh-size dependency in numerical simulations of reinforced concrete (RC) structures subjected to blast loading. A tensile failure criterion that can minimize the mesh-dependency of simulation results is introduced based on the fracture energy theory. In addition, conventional plasticity based damage models for concrete such as the CSC model and the HJC model, which are widely used for blast analyses of concrete structures, are compared with the orthotropic model that adopts the introduced tensile failure criterion in blast tests to verify the proposed criterion. The numerical predictions of the time-displacement relations at the mid-span of RC beams subjected to blast loading are compared with experimental results. The analytical results show that the numerical error according to the change in the finite element mesh size is substantially reduced and the accuracy of the numerical results is improved by applying a unique failure strain value determined by the proposed criterion.

Keywords: tensile criterion; high strain rate concrete; blast simulation; fracture energy; mesh-dependency

1. Introduction

In the context of increasing demand to ensure the stability of concrete structures against the threat of bombing terror, understanding the behavior of RC structures subjected to blast loading is an important research topic. Accordingly, numerous studies ranging from modelling concrete material properties to analysis of RC structures subjected to blast loading have been carried out (Hao *et al*. 2012, Zhang *et al*. 2014). Under blast loading conditions, concrete shows different behavior from that in a quasi-static condition, and this difference becomes greater as the strain rate increases (Cusatis 2011). Moreover, concrete develops a broad distribution of internal micro-cracks preceding crushing and cracking in the process of fracture and exhibits different behavior according to the combinations of stress states (Kwak and Song 2002). Hence, the characteristics of concrete caused by strain rate and multi-axial effects must be considered to predict the response of concrete structures under blast loading.

Mathematical concrete models such as the CSC (Continuous Surface Cap), HJC (Holmquist Johnson Cook), and K&C (Karagozian & Case) models (Holmquist and Johnson 1993, Schwer and Malvar 2005, Murray 2007), which consider both the strain rate effect and the confining pressure effect, are widely used in the numerical analyses of concrete structures subjected to blast loading. Upon the adoption of a mathematical concrete model, blast analyses for concrete structures are conducted. Since the blast loading usually causes nonlinear deformations induced by the cracking of concrete, the blast analyses of concrete structures must be based on the use of a crack model. To this end, a smeared crack model, representing cracked concrete as an elastic orthotropic material with a reduced elastic modulus in the direction perpendicular to the crack plane, is widely used to describe the nonlinear behavior of concrete structures because of its simplicity and computational efficiency. Nevertheless, it has a major drawback of mesh-size and mesh-bias dependency in numerical results (Cevera and Chiumenti 2006), and this drawback is not limited to the quasi-static conditions but is observed identically in high strain rate conditions such as blast and impact loadings (Georgin and Reynouard 2003). The numerical results of concrete structures consequently may vary depending on the change in the FE mesh size (Kwak and Gang 2015), and the accuracy of numerical results may not be guaranteed. In efforts to resolve this mesh dependency problem, various studies have been carried out, from the introduction of a viscoplastic model (Sluys and De Borst 1992) to the adoption of a mesh-free method (Rabczuk and Eibl 2006).

Nevertheless, no guideline or criterion to reduce the mesh dependency of numerical results in simulations of concrete structures subjected to high strain rate loading has been introduced. As a result, the FE mesh size is entirely determined by the empirical judgement of the researchers. In contrast with the impact loading by a projectile, where a guideline or criterion related to the compression failure has been recognized as a significant issue (Kwak and Gang 2015), blast loading warrants greater attention with respect to the tension failure of concrete structures. In this context, since the target structures mainly investigated in this paper are RC beam subjected to blast loading, the stress-strain

*Corresponding author, Professor
E-mail: khg@kaist.ac.kr

http://www.techno-press.org/?journal=cac&subpage=8
ISSN: 1598-8198 (Print), 1598-818X (Online)

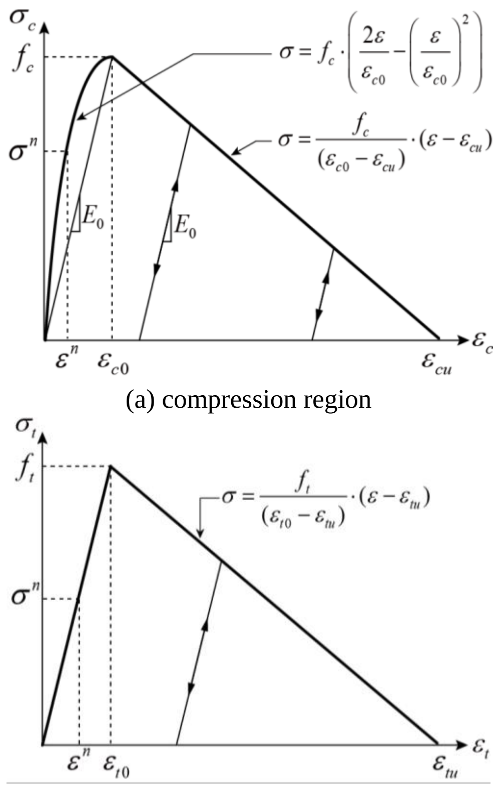

(b) tensile region

Fig. 1 Stress-strain relation of concrete

relation under tensile failure is of primary interest. Upon this background, this paper introduces a tension failure criterion to minimize the mesh-dependency of simulation results based on the fracture energy theory, and the corresponding tensile failure (ultimate) strain value in the stress-strain relation is calculated by the criterion whenever the FE mesh size is changed. Moreover, the introduced tensile failure criterion is implemented into the nonlinear elastic orthotropic model (Gang and Kwak 2017), which was proposed to depict the structural response of concrete subjected to blast or impact loading, and the reliability of the proposed criterion is examined by comparing the numerical prediction with experimental results (Seabold 1970, Magnusson and Hallgren 2003) obtained by blast tests of RC beams.

2. Material properties

To predict the nonlinear behavior of reinforced concrete (RC) structures subjected to blast loading, the definition of the stress-strain relation must be preceded. Among the numerous mathematical models currently used in defining the stress-strain relation of concrete, this paper adopts the monotonic uniaxial stress-strain relation proposed by Scott *et al*. (1982) which can describe nonlinear strain hardening before peak strengths of f_c and f_t, respectively and then linear softening up to the failure (ultimate) strain of ε_u (see Fig. 1). In this model, failure will occur when the strain exceeds the ultimate strain values of ε_{cu} or ε_{tu}. Differently from concrete in the compression region where crushing is considered, if any strain of two principal strains exceeds the ultimate strain value, concrete in tension is assumed to lose its resistant capacity in the orthogonal direction to the developed crack only. Concrete in tension maintains its resisting capacity until the strains in the both the principal strain axes exceed the ultimate strain values of ε_{tu}. The corresponding ultimate strain values of ε_{cu} and ε_{tu} are determined by the compressive failure criterion proposed by Kwak and Gang (2015) and the tensile failure criterion introduced in this paper respectively.

Upon the description of the monotonic envelope curve, the unloading-reloading paths must be defined to depict the hysteretic behavior of concrete. Although unloading and reloading follow nonlinear paths, which together from a hysteretic loop, this paper does not take into account these nonlinear paths because of their minor influence on the hysteretic response of the structure but rather adopts a straight unloading-reloading path parallel to the secant modulus in the compression and tension region for computational convenience (see Fig. 1) (Fujikake *et al*. 2009).

Under blast loading conditions, concrete material properties are quite different from that in a quasi-static condition. Due to the lateral inertia confinement and the change of the crack pattern (Gang and Kwak 2017), significant increases in the compressive and tensile strengths f_c and f_t together with increases of ε_{c0} and ε_{t0} are expected. More details of concrete material properties at high strain rates can be found in previous studies (Li and Meng 2003, Lu and Li 2011). In order to estimate these changes in the material properties of concrete according to the strain rate, various mathematical models (Shkolnik 2008, Tu and Lu 2010) have been introduced and used in the numerical analyses of RC structures. Nevertheless, simple equations have been used in this paper to determine the uniaxial dynamic compressive and tensile strengths of concrete on the basis of the relations used by Gang and Kwak (2017) and the CEB-FIP Model Code (1993) respectively, as shown in Eqs. (1) and (2). The dynamic compressive and tensile strength f_c^{dyn} and f_t^{dyn} determined from Eqs. (1) and (2) will replace the static compressive and tensile strength f_c and f_t in Fig. 1.

$$\frac{f_c^{dyn}}{f_c} = \left[A + B\left(P^*\right)^N \right]\left[1 + C\ln\left(\dot{\varepsilon}_c^{dyn}\right)\right] \tag{1}$$

$$\frac{f_t^{dyn}}{f_t} = \left(\frac{\dot{\varepsilon}_t^{dyn}}{\dot{\varepsilon}_t}\right)^{\delta} \quad \dot{\varepsilon}_t^{dyn} \le 30s^{-1}, \qquad \frac{f_t^{dyn}}{f_t} = \beta\left(\frac{\dot{\varepsilon}_t^{dyn}}{\dot{\varepsilon}_t}\right)^{\frac{1}{3}} \quad \dot{\varepsilon}_t^{dyn} \ge 30s^{-1} \tag{2}$$

where *A*, *B*, *C*, and *N* are material constants determined by a SHPB (Split Hopkins Pressure Bar) test for strain rates ranging from 100/s to 800/s. f_c^{dyn} and f_t^{dyn} represent the dynamic compressive and tensile strength in MPa, and f_c and f_t represent the static compressive and tensile strength in MPa, respectively. Moreover, $\delta = (1+8f_c/10\text{Mpa})^{-1}$, $\log\beta = 6\delta - 2$, $\dot{\varepsilon}_t = 10^{-6}s^{-1}$ and $\dot{\varepsilon}_c^{dyn}$ and $\dot{\varepsilon}_t^{dyn}$ denote the corresponding compressive and tensile strain rates. More details including equations and material constants can

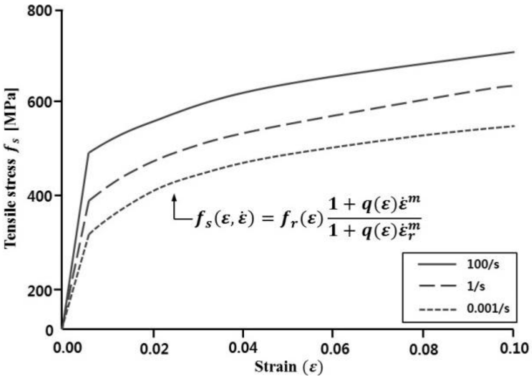

Fig. 2 Stress-strain relation of steel according to the strain rate

be found in the CEB-FIP model code (1993) and a previous study (Gang and Kwak 2017).

Since reinforcing steel generally presents identical material properties for compression and tension region, the same stress-strain curve has been adopted to trace the behavior of reinforcing steel under compression and tension. The changes in material properties of reinforcing steel with strain rate are similar to those of concrete. The yield strength and the ultimate strength of steel increases with increasing strain rate (Lin *et al*. 2008). Among many dynamic stress-strain relations of steel proposed on the basis of experimental studies (Sung *et al*. 2010, Peirs *et al*. 2011), the relation in Fig. 2 is used in this paper because of its simplicity (Lim *et al*. 2013), where $q(\varepsilon) = 0.0746(\varepsilon + 0.00285)^{-0.662}$, $m(\varepsilon) = 0.184(\varepsilon + 0.0015)^{0.0755}$, and $f_r(\varepsilon)$ denotes the stress at the semi-static strain rate of $\dot{\varepsilon}_r = 0.003s^{-1}$. More details of the stress-strain relation can be found in a previous study (Lim *et al*. 2013).

Upon the definition of the dynamic stress-strain relation of steel, the unloading-reloading paths need to be defined as well, and a straight unloading-reloading path parallel to the elastic modulus has been assumed because of its minor effect on the maximum response in a RC beam subjected to blast loading.

3. Definition of strength envelope

In order to describe the multi-axial behavior of concrete under blast loading, not only the uniaxial stress-strain relation of concrete but also the strength envelope of concrete should be defined, and many mathematical concrete models such as the CSC (Continuous Surface Cap) and HJC (Holmquist Johnson Cook) are currently used to simulate the multi-axial behavior of concrete with the strength envelope. However, all the models are plastic based models, which cannot adequately trace the strain softening behavior of concrete beyond the peak stress. Because of the limitation of plastic based models in describing the strain softening behavior of concrete, an elastic based orthotropic model (Gang and Kwak 2017) was proposed by the authors and has been adopted to simulate the multi-axial behavior of RC beams subjected to blast loading in this paper.

Since the strength enhancement of concrete in biaxial stress states is attributed to both the strain rate and the lateral confining pressure, both factors should be considered in the strength envelope of concrete in biaxial stress states. Based on correlation studies between experimental results (Yan and Lin 2007) and associated parametric studies, Gang and Kwak (2017) introduced the simple expression in Eq. (3) to evaluate the dynamic strength of concrete in a biaxial compressive stress state.

$$R(\alpha) = \frac{f_d}{f_s} = P_1 + \frac{P_2}{(1+\alpha)^2} + \frac{P_3\alpha}{(1+\alpha)^2} \qquad (3)$$

where f_d and f_s are the dynamic strength of concrete in a biaxial stress state and the uniaxial strength of concrete under quasi-static loading, $\alpha=\sigma_1/\sigma_2$ $\left(|\sigma_1| \geq |\sigma_2|\right)$ is the principal stress ratio, and P_1, P_2, and P_3 represent parameters associated with material properties. By fitting to the test data, P_1, P_2, and P_3 were determined as -0.446, 1.446 and 6.42, respectively, and Eq. (3) shows good agreement with the test data for the change of the strain rate (Gang and Kwak 2017).

The strain rate effect was considered while defining the dynamic uniaxial compressive strength, and the HJC model of $g(\dot{\varepsilon}) = \left(A + BP^{*N}\right)\left(1 + C\ln(\dot{\varepsilon}^*)\right)$ is adopted in this paper upon determining the material constants *A*, *B*, *C*, and *N* through an experiment that consists of the SHPB (Split Hopkins Pressure Bar) test for strain rates ranging from 100/s to 800/s, where $g(\dot{\varepsilon}) =$ the dynamic increase factor for the uniaxial compressive strength (see Fig. 3), $P^* =$ normalized pressure for uniaxial stress state, and $\dot{\varepsilon}^* =$ normalized strain rate (Gang and Kwak 2017). The equation defined in the HJC model has only been used to determine the dynamic uniaxial compressive strength of concrete with respect to the change of the strain rate. The use of the HJC model makes it possible to accurately estimate the dynamic compressive strength of concrete because the four material constants of *A*, *B*, *C*, and *N* depending on the used material can uniquely and directly be determined through the SHPB test. Since the HJC model with the material constants used in this paper shows good agreement with the CEB-FIP code formulated on the basis of the experiment in a range from 10^{-5}/s to 100/s, the HJC model has been adopted instead of the CEB-FIP code to trace the uniaxial strength of concrete in a higher range of strain rates (Gang and Kwak 2017).

Upon verifying the biaxial strength envelope and the stress-strain relation for the two principal stress components σ_1 and σ_2, the other stress component σ_3 must additionally be considered to represent the complete three-dimensional strength envelope. Gang and Kwak (2017) introduced another function $h(\sigma_3/f_c)$ given as Eqs. (4) and (5) to take into account the triaxial stress effect.

$$h(\sigma_3, f_c) = 3.13\frac{\sigma_3}{f_c} + 1 \ (\sigma_3 \leq 0) \qquad (4)$$

$$h(\sigma_3, f_c) = 7.137\frac{\sigma_3}{f_c} + 1 \ (\sigma_3 > 0) \qquad (5)$$

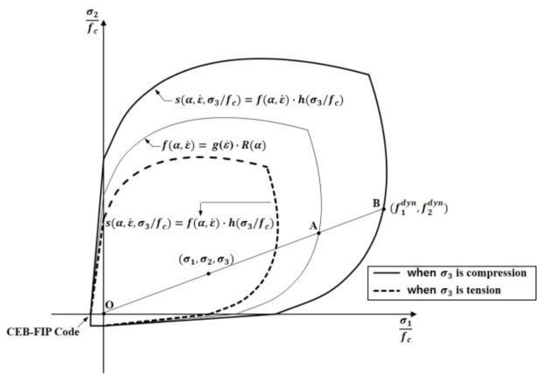

Fig. 3 Triaxial strength envelope of strain rate dependent orthotropic model

Accordingly, the multiplication of $h(\sigma_3/f_c)$ by the equation for the biaxial strength envelope $f(\alpha,\dot{\varepsilon}) = g(\dot{\varepsilon}) \cdot R(\alpha)$ finally represents the triaxial strength envelope of concrete in the triaxial compression region (see $s(\alpha,\dot{\varepsilon},\sigma_3/f_c) = h(\sigma_3/f_c) \cdot f(\alpha,\dot{\varepsilon})$ in Fig. 3). As shown in previous research (Gang and Kwak 2017), the triaxial strength envelope used in this paper presents good agreement with experimental data.

Although a unique strength envelope has been introduced to define the compression-compression region on the basis of experimental data, no experiments have been carried out to define the triaxial strength envelope in the compression-tension and tension-tension regions. In this context, as was adopted in the compression-tension region under a biaxial stress state (Gang and Kwak 2017), the linear relation connecting the dynamic uniaxial compressive strength and the tensile strength has been used in this paper (see Fig. 3). Since no change of the strength envelope has been assumed in the triaxial tension region, the dynamic uniaxial tensile strength has been used to define the triaxial tension region. Fig. 3 shows the finally constructed triaxial strength envelope (Gang and Kwak 2017).

4. Development of tensile failure criterion

Fracture in concrete depends to a large extent on the material properties in tension and the strain-softening behavior induced by the occurrence and propagation of internal micro-cracks. In this process of fracture in concrete, microcracks develop and form a fracture process zone which manifests as strain softening. This strain softening behavior leads to fracture of concrete when the microcracks coalesce to form a single continuous macrocrack and stress in the zone reduces to zero. This distribution pattern of internal microcracks varies depending on the size of the specimens. When the size of the specimen is small, the microcracks are uniformly distributed in the specimen, while the microcracks are concentrated in a smaller cracked region of the specimen when the size of the specimen is relatively large (Kwak and Filippou 1990). This means that development of fracture patterns may vary depending on the change in the size of the specimens even in the same type of concrete, and these characteristics must be considered in the

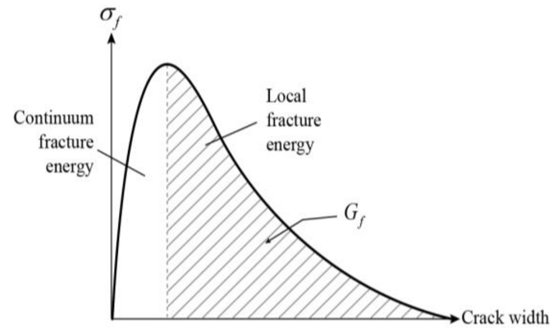

(a) Configuration

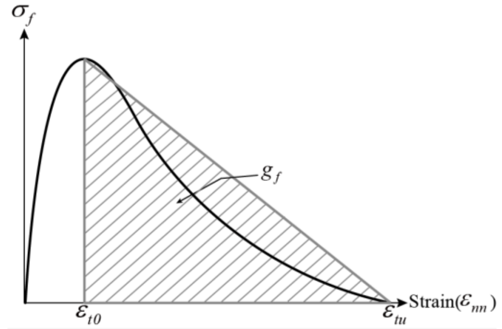

(b) Idealization

Fig. 4 Expression of fracture energy

numerical analyses of RC structures whose cracking behavior has been described based on the smeared crack model (Cervera and Chiumenti 2006).

In order to simulate this strain softening behavior of concrete in tension, many models have been proposed and used in the analyses of concrete structures subjected to blast loading which accompanies the tension failure (Hillerborg *et al*. 1976, Bažant and Oh 1983). Failure strains determined by these proposed models have been used in the analyses of concrete structures and show very satisfactory results when the FE mesh size is relatively small. However, the results of numerical analyses are quite different from experimental data when the FE mesh size becomes large. The reason for this numerical error is that the proposed models assume a uniform distribution of microcracks over the fracture zone in an element while microcracks are in fact concentrated in a much smaller cracked region of the element.

Upon this background, a new tensile failure criterion that can reduce numerical error caused by the mesh-dependency problem has been introduced in this paper, and its formulation starts from the fracture energy theory. As shown in Fig. 4(a), the fracture energy of concrete can be divided into two parts, the continuum fracture energy corresponding to the strain hardening region and the local fracture energy corresponding to the strain softening region and more attention is given to the local fracture energy of concrete in the tension region. The local fracture energy G_f defined as the amount of energy dissipated to crack one unit of area in a continuous crack can be expressed as the area under the strain softening region in Fig. 4(a).

$$G_f = \int \sigma_f \cdot dw \tag{6}$$

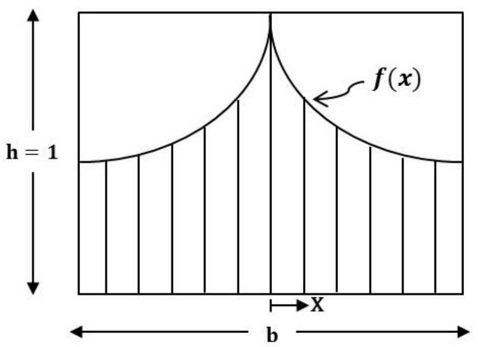

Fig. 5 Assumed distribution of micro-crack in an element

where w represents the sum of the opening displacements of all microcracks within the fracture zone and can be expressed as the accumulated crack strain in the smeared crack model, which means $w=\int \varepsilon_{nn} \cdot dn$. If it is assumed that the micro-cracks are uniformly distributed across the fracture zone, this equation can be reduced to $w=b \cdot \varepsilon_{nn}$ and the fracture energy can be expressed as $G_f=g_f \cdot b$, where b denotes the FE mesh size, and the area g_f under the curve in Fig. 4(b) can be expressed as $g_f=\int \sigma_f d\varepsilon_{nn}$.

However, the relation between G_f and g_f should be modified when a relatively large finite element size is used for numerical analyses. In order to consider that the microcracks are concentrated in a fracture process zone that may be small compared to the size of the finite element, a function $f(x)$ that represents the distribution of microcracks across the element width is introduced in this paper (see Fig. 5). On the basis of the introduction of the function $f(x)$, the relation between the fracture energy G_f and the area under the entire softening stress-strain curve g_f can be expressed as $G_f=g_f \cdot \int_b f(x)dx$. This can then be expressed by Eq. (7) with an assumption of linear strain softening behavior in concrete, as shown in Fig. 4(b), where ε_{t0} and ε_{tu} are the strains corresponding to the tensile strength of concrete f_t, and a failure condition that characterizes the end of the strain softening region when the microcracks coalesce into one continuous macrocrack.

$$G_f=g_f \cdot \int_b f(x)dx=\frac{1}{2}(\varepsilon_{tu}-\varepsilon_{t0}) \cdot f_t \cdot \int_b f(x)dx \tag{7}$$

The distribution function is defined with a general exponential function $f(x)=\alpha \cdot e^{\beta \cdot x}$ to represent the concentration of microcracks near the crack tip when the finite element mesh size becomes fairly large (Kwak and Filippou 1990) (see Fig. 5). The use of boundary conditions $f(0)=1.0$ and $f(b/2)=(b_0/b)^{\gamma}$ produces the following equation for the distribution function

$$f(x)=e^{-2/b \cdot \gamma \cdot \ln(b/b_0) \cdot x} \tag{8}$$

where b=the element width, b_0=the reference value for the maximum element width at which a uniform distribution of micro-cracks can be expected, and b_0=6 mm is used in this paper on the basis of the experimentally determined value (Vonk 1993). Moreover, γ represents an experimental

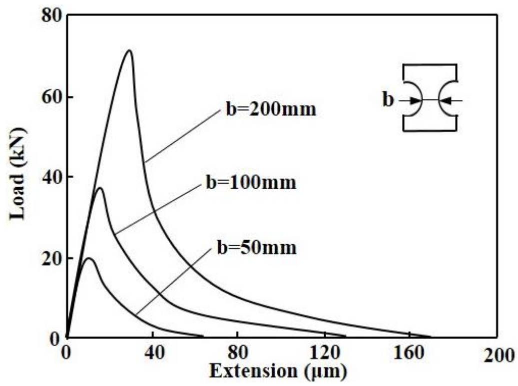

Fig. 6 Experimental load-extension curves of specimens (Carpinteri and Ferro 1994)

constant obtained from the tensile fracture test of concrete specimens. The substitution of Eq. (8) into Eq. (7) gives the following equation for the tensile failure strain ε_{tu}.

$$\varepsilon_{tu}=\frac{2 \cdot G_f \cdot \gamma \cdot \ln(\frac{b}{b_0})}{f_t \cdot \left(\left(\frac{b}{b_0}\right)^{\gamma}-1\right) \cdot b_0}+\varepsilon_{t0} \tag{9}$$

In Eq. (9), the experimental constant has been determined through a regression analysis of the experimental data (Carpinteri and Ferro 1994, Van Vliet and Van Mier 2000, Roesler *et al*. 2007). A description of the load-extension curve obtained from the fracture test is provided in Fig. 6. In order to find the value of the tensile failure strain with respect to the specimen size, load versus extension curves in Fig. 6 should be converted to stress-strain curves and then normalized for the test data corresponding to b=50 mm. The normalization process was carried out in order to exclude the effect caused by the strength of the specimen and to reflect only the size effect on the proposed failure criterion. The same procedure has also been peformed for the test data obtained by Van Vliet and Van Mier (2000). Finally, the converted failure strains ε_{tu} and tensile strengths f_t corresponding to each specimen of concrete are given in Table 1. A scatter diagram for the tensile failure strain ε_{tu} according to the specimen size can be constructed as shown in Fig. 7 and then a regression analysis has been performed to determine the material constant γ. Since the experiment results show that G_f/f_t can be considered as a constant value regardless of the size of the concrete specimens (Wittmann *et al*. 1988), the constructed function ε_{tu} in Eq. (9) may be considered to be independent of the concrete type. Fig. 7 shows the scatter diagram and corresponding regression relation for ε_{tu} introduced in this paper. The reference value for the critical strain ε_{t0} is assigned as ε_{t0}=0.00015, and tensile strength f_t=4.25 MPa and fracture energy G_f=0.083 N/mm have been used for the regression analysis. In advance, as shown in Fig. 7, the material constant γ=2.1 has been determined by a regression analysis for the tensile fracture test of concrete specimens (Carpinteri and Ferro 1994, Van Vliet and Van Mier 2000, Roesler *et al*. 2007) to be the most suitable value. If b is equal to 6 mm, then a uniform distribution of

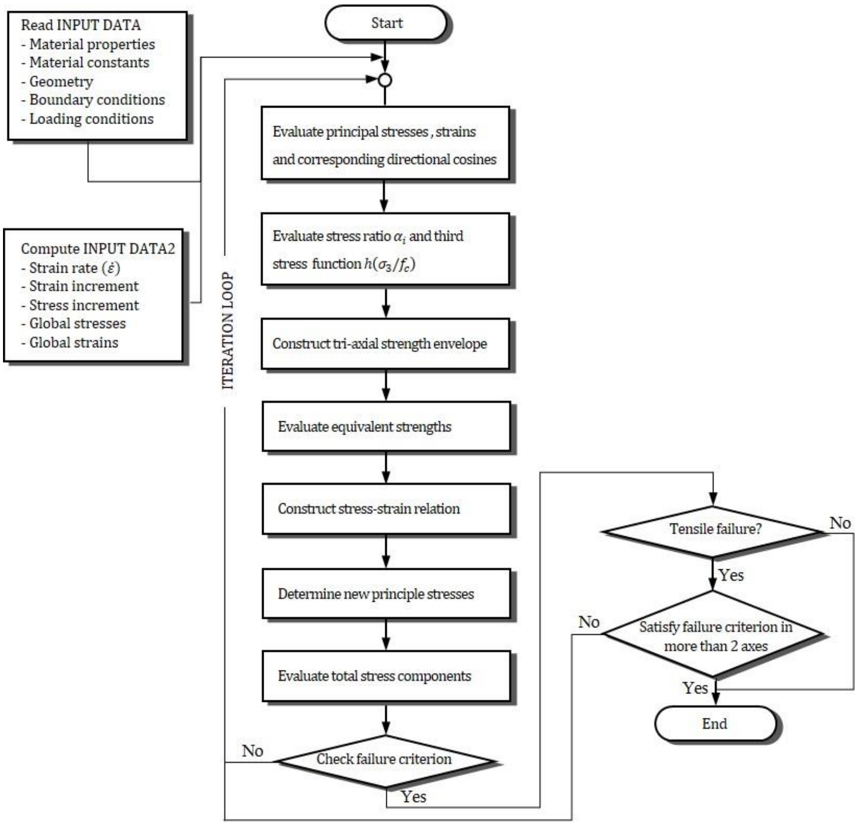

Fig. 8 The solution procedure of the strain rate dependent orthotropic model

Table 1 Measured failure strains and material constants of specimens (Carpinteri and Ferro 1994, Van Vliet and Van Mier 2000, Roesler *et al*. 2007)

Specimen width (mm)	Tensile strength (MPa)	Failure strain
21	4.15	0.001398
30	2.17	0.000782
50	4.25	0.000415
60	2.23	0.000521
100	3.78	0.00029
120	2.48	0.000351
200	3.64	0.000187
240	2.37	0.000229

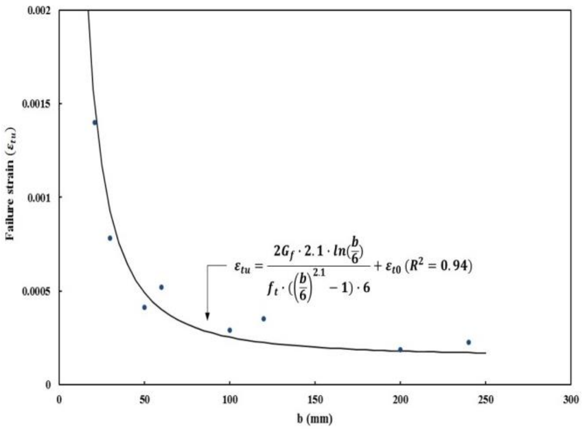

Fig. 7 Regression analysis for ε_{tu}

microcracks across the finite element width is assumed, and hence the expression of ε_{tu} can be simplified as $\varepsilon_{tu} = \frac{G_f}{3 \cdot f_t} + \varepsilon_{t0}$. With an increase of the finite element mesh size, however, the value of ε_{tu} is decreased. This approach for defining ε_{tu} renders the analytical solution insensitive to the mesh size and improves the accuracy of the numerical results.

Upon defining the tensile failure strain, the strain rate effect must additionally be considered to introduce a tensile failure criterion that can minimize the mesh-dependency in the numerical analyses of concrete structures subjected to blast loading that accompanies strain rate deformation. As shown in previous experimental studies (Zhang *et al*. 2009), an increase of the strain rate causes an increase of the tensile strength of concrete f_t as well as an increase of the local fracture energy G_f.

To take into account the strain rate effect, the DIF (Dynamic Increase Factor) equation for G_f/f_t has been adopted from the experimental data (Zhang *et al*. 2009). Sine DIFs for tensile strength and fracture energy have respectively been expressed as the function of strain rate, as shown in Eqs. (10) and (11), the substitution of DIF into the equation of the tensile failure strain ε_{tu} in Eq. (9) finally represents the tensile failure criterion to be used in the numerical analyses of concrete structures subjected to blast loading. However, because of the limitation of the test specimen in obtaining Eqs. (10) and (11), the use of the introduced Eqs. (12) and (13) should be restricted to a finite element mesh size larger than 20 mm.

Table 2 Material properties of the RC beams

Specimens	fc (MPa)	f_y (MPa)	E_c (GPa)	E_s (GPa)	Reinforcement
WE5	27	470	27.8	200	2 No.7 / 2 No.9
B40-D1	43	604	31.5	210	5ϕ16 mm

Table 3 Information of blast loadings

Specimens	Q (kg)	p_r (MPa)	i (kPa s)
WE5	-	414	-
B40-D1	1.1	650	3.76
	Mass of explosive charge	Maximum reflected pressure	Impulse density

$$\frac{G_f^{dyn}}{G_f} = 1 + 0.7438(\dot{\varepsilon})^{0.17} \quad \dot{\varepsilon} < 7.04s^{-1} \tag{10}$$

$$\frac{G_f^{dyn}}{G_f} = -179 + 63.7 \cdot (2 + \log(\dot{\varepsilon})) \quad \dot{\varepsilon} \geq 7.04s^{-1} \tag{11}$$

$$\varepsilon_{tu} = \frac{4.2G_{f(static)} \cdot \ln(\frac{b}{6}) \cdot (1 + 0.7438(\dot{\varepsilon})^{0.17})}{6 f_{t(static)} \cdot \left(\left(\frac{b}{6} \right)^{2.1} - 1 \right) \cdot (1 + 1.047(\dot{\varepsilon})^{0.51})} + \varepsilon_{t0} \quad \dot{\varepsilon} < 7.04s^{-1} \tag{12}$$

$$\varepsilon_{tu} = \frac{4.2G_{f(static)} \cdot \ln(\frac{b}{6}) \cdot (-179 + 63.7 \cdot (2 + \log(\dot{\varepsilon})))}{6 f_{t(static)} \cdot \left(\left(\frac{b}{6} \right)^{2.1} - 1 \right) \cdot (1 + 1.047(\dot{\varepsilon})^{0.51})} + \varepsilon_{t0} \quad \dot{\varepsilon} \geq 7.04s^{-1} \tag{13}$$

5. Solution procedure

Upon defining the tensile failure strain and the triaxial ultimate strength envelope, the sequential solution steps of the orthotropic concrete model (Gang and Kwak 2017) should be introduced for application of the proposed failure criterion to blast analyses. A summary of the solution procedure for the evaluation of stresses is presented in Fig. 8 and more details of the solution steps along with the corresponding operations can be found in a previous study (Gang and Kwak 2017). The description in Fig. 8 is related to the application of the failure criterion within an element.

6. Numerical analysis

To verify the accuracy of the proposed criterion in predicting structural behavior under blast loading, numerical analyses have been conducted for the WE5 RC beam tested by Seabold (1970) and B40-D1 tested by Magnusson and Hallgren (2000) using LS-DYNA 971 (2007) along with a comparison of the numerical results to the concrete damage models CSC (Type 159 in LS-DYNA) and HJC (Type 111 in LS-DYNA) and an orthotropic model (Gang and Kwak 2017) that adopts the introduced tensile failure criterion. The material properties of the specimens are summarized in Table 2 and information of the applied blast loadings used in the numerical analyses is presented in Table 3. More details including the experimental setup can be found elsewhere (Magnusson and Hallgren 2000).

The geometric configuration and the loading history of the WE5 RC beam are represented in Figs. 9 and 10. Blast loading is assumed to be applied to the RC beam as a

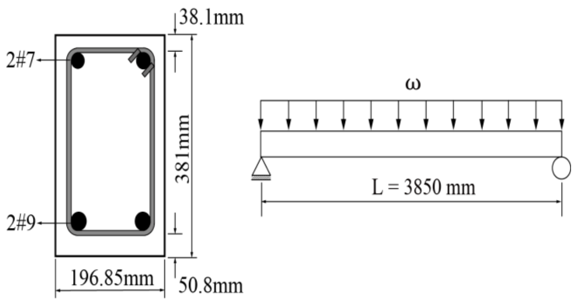

Fig. 9 Geometric configuration of WE5 RC beam

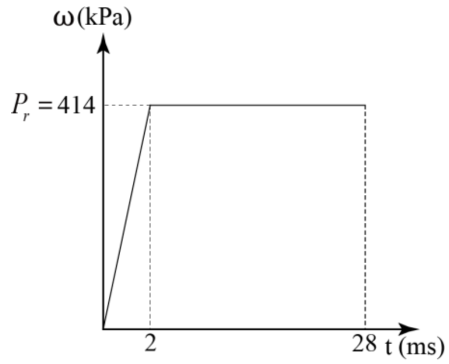

Fig. 10 Loading history of WE5 RC beam

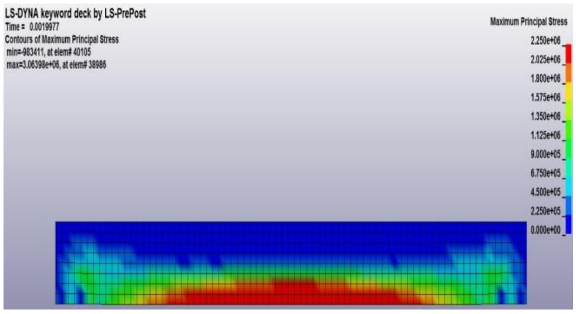

(a) t=2ms

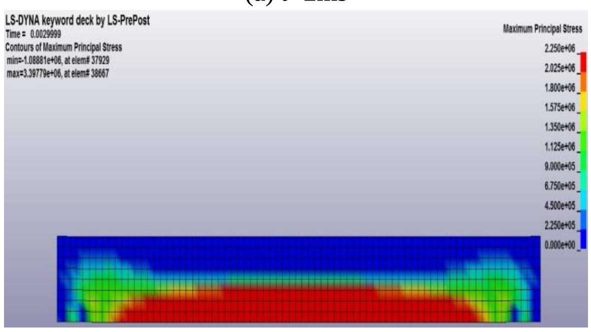

(b) t=3ms

Fig. 11 Initial stress distribution during blast analyses

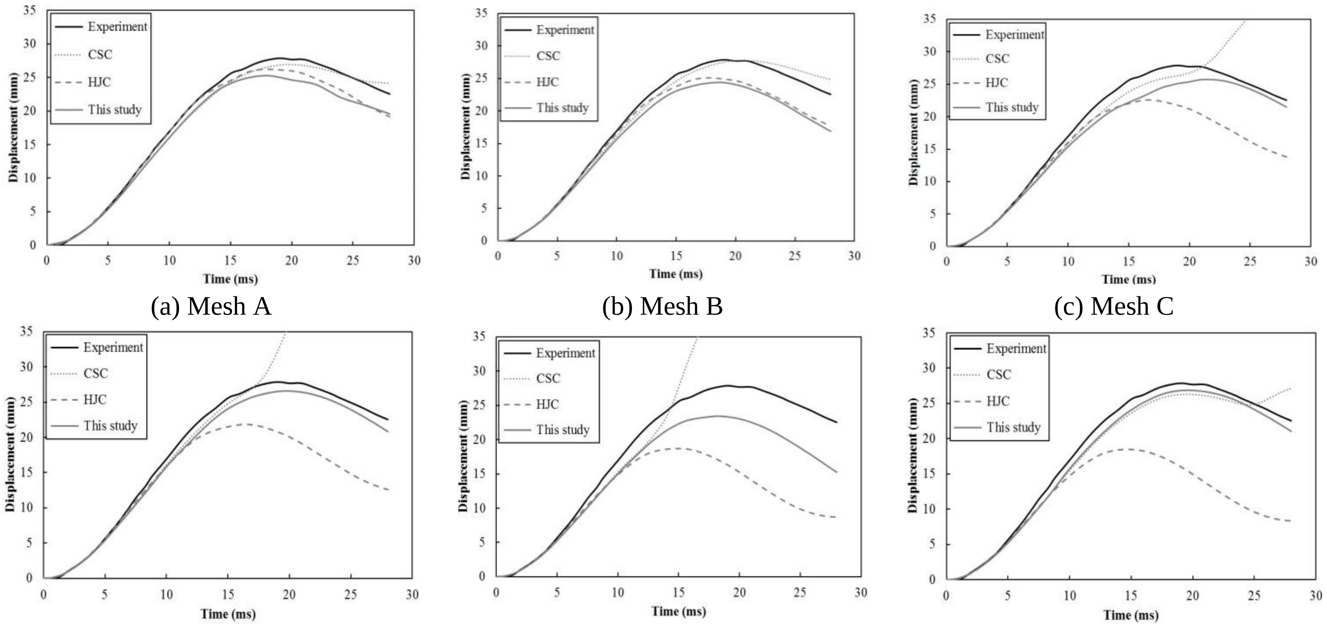

(a) Mesh A (b) Mesh B (c) Mesh C

(d) Mesh D (e) Mesh E (f) Mesh F

Fig. 12 Time-displacement relation of WE5 RC beam

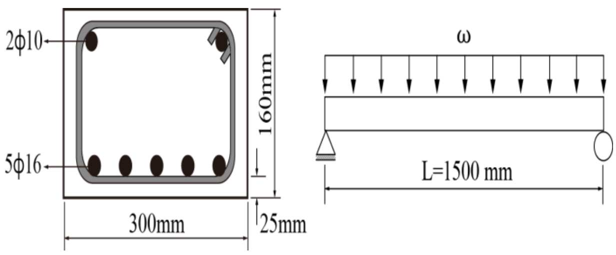

Fig. 13 Geometric configuration of B40-D1 RC beam

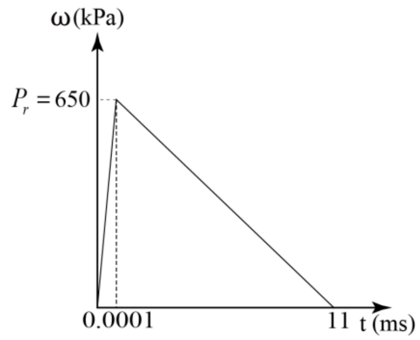

Fig. 14 Loading history of B40-D1 RC beam

uniformly distributed loading. The numerical prediction of the time-displacement relation at the mid span of the RC beam has been compared with experimental results. Furthermore, to examine efficiency of the proposed failure criterion in reducing the mesh dependency of the numerical results, six different size of cubic solid elements with dimensions of 10 mm (Mesh A), 20 mm (Mesh B), 30 mm (Mesh C), 40 mm (Mesh D), 50 mm (Mesh E), and 60 mm (Mesh F) are applied for the FE discretization of concrete, Furthermore, the reinforcing steel placed in concrete is modelled with a one-dimensional truss model constrained in solid elements, which is usually adopted in the modeling of reinforcing steel (Unosson and Nilsson 2006). Figs. 11(a)-(b) show the initial stress distributions of the reinforced beam obtained from the blast analyses. The color of the fringe indicates the level of tensile stress distribution (principal stress) during the blast analyses. For concrete in tension, when the color of the fringe is close to red, it means that the concrete is cracking. As can be seen, the cracks of the concrete beam initiate in the center area on the bottom surface, and then they propagate quickly with cracks found in the support area on the bottom surface (Lin *et al*. 2014).

Figs. 12(a) to (f) present a comparison of the experimental results with the numerical predictions of the time-displacement relation at the mid-span of the WE5 RC beam. Numerical results of this study in Fig. 12 are obtained by the use of the orthotropic model, which adopts a tensile failure strain value determined by the proposed criterion. As shown in these figures, the CSC model shows good agreement with the experimental data when a relatively small mesh size is used for the numerical analyses. Meanwhile, numerical results of the orthotropic model (Gang and Kwak 2017) that adopts the introduced failure criterion gives satisfactory agreement with the experimental results through the entire range of the FE mesh size considered in this study.

The second beam is B40-D1 and the geometric configuration and the loading history of a RC beam for B40-D1 are respectively represented in Figs. 13 and 14. A shock wave of blast loading propagated uniformly through the shock tube, because the tube prevented the wave from expanding spherically (Magnusson and Hallgren 2003). In this context, blast loading is assumed to be applied to the RC beam as a uniformly distributed loading.

Numerical analyses of the same procedure have been carried out for the B40-D1 RC beam. Figs. 15(a) to (f) present a comparison of the experimental results with the numerical predictions of the time-displacement relation at the mid-span of the B40-D1 RC beam. As shown in these

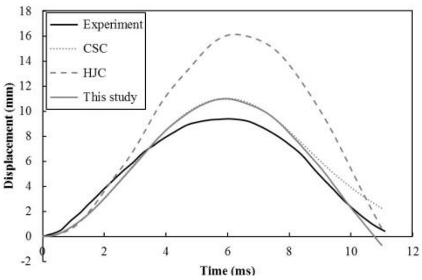

(a) Mesh A

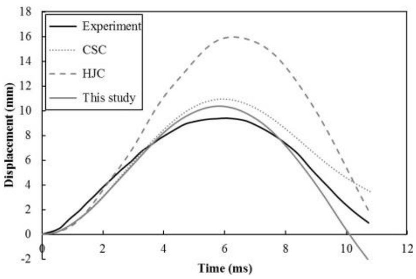

(b) Mesh B

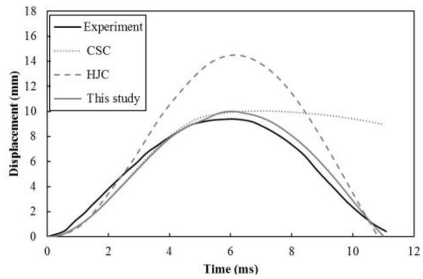

(c) Mesh C

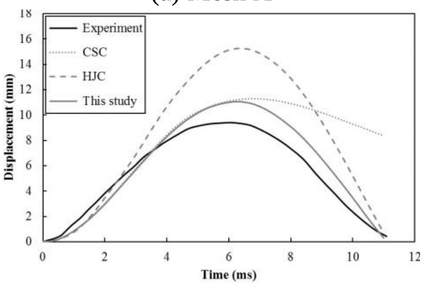

(d) Mesh D

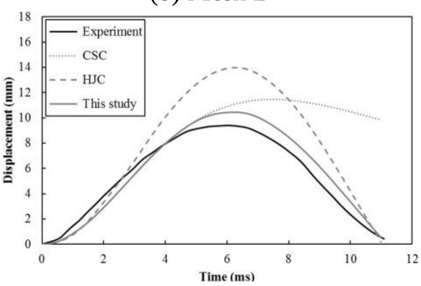

(e) Mesh E

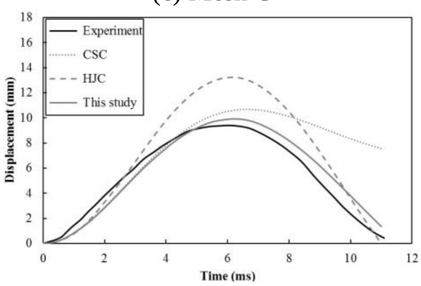

(f) Mesh F

Fig. 15 Time-displacement relation of B40-D1 RC beam

figures, application of the orthotropic model that adopts the introduced failure criterion to the blast analyses gives not only very satisfactory agreement between the numerical and the experimental results but also shows less sensitivity to the variation of the FE mesh size used in the numerical analyses. Upon the obtained results for the blast analyses of concrete structures, it can be concluded that the proposed tensile failure criterion can effectively be used to trace the structural responses of RC structures that accompany strain rate dependent deformation regardless of the FE mesh size that is used.

7. Conclusions

This paper introduces a tensile failure criterion that can minimize the mesh dependency in numerical analyses of RC structures based on the fracture energy theory. The introduced criterion is applied to blast analyses to examine its efficiency in reducing the mesh dependency of the numerical results, and its accuracy in tracing the behavior of a RC beam subjected to a blast loading. A Comparison between the numerical and the experimental results shows that the numerical error caused by the mesh-dependency problem is reduced substantially and the accuracy of the simulation results is reliable when the tensile failure strain value determined by the introduced criterion is applied to blast analyses. In conclusion, the introduced failure criterion can effectively be used in blast analyses to obtain reliable results regardless of the FE mesh size that is employed.

Acknowledgments

This research was supported by a Construction Technology Research Project (17SCIP-B128706-01) and a grant(13SCIPA02) from Smart Civil Infrastructure Research Program funded by Ministry of Land, Infrastructure and Transport(MOLIT) of Korea government and Korea Agency for Infrastructure Technology Advancement(KAIA).

References

Bažant, Z.P. and Oh, B.H. (1983), “Crack band theory for fracture of concrete”, *Mater. Struct.*, **16**(3), 155-177.

Carpinteri, A. and Ferro, G. (1994), “Size effects on tensile fracture properties: A unified explanation based on disorder and fractality of concrete microstructure”, *Mater. Struct.*, **27**(10), 563-571.

Cevera, M. and Chiumenti, M. (2006), “Smeared crack approach: Back to the original track”, *J. Numer. Anal. Meth. Geomech.*, **30**(12), 1173-1199.

Comite Euro-International De Beton (1993), *CEB-FIP Model Code 1990*, Redwood Books, Wiltshire, U.K.

Cusatis, G. (2011), “Strain-rate effects on concrete behavior”, *J. Impact Eng.*, **38**(4), 162-170.

Fujikake, K., Li, B. and Soeun, S. (2009), “Impact response of reinforced concrete beam and its analytical evaluation”, *J. Struct. Eng.*, **135**(8), 938-950.

Gang, H.G. and Kwak, H.G. (2017), “A strain rate dependent orthotropic concrete material model”, *J. Impact Eng.*, **103**, 211-224.

Georgin, J.F. and Reynouard, J.M. (2003), “Modeling of structures subjected to impact: Concrete behaviour under high strain rate”, *Cement Concrete Compos.*, **25**(1), 131-143.

Hallquist, J.O. (2007), *LS-DYNA Keyword User’s Manual (Version 971)*, Livermore Software Technology Corporation, California, U.S.A.

Hao, Y., Hao, H. and Zhang, X. (2012), “Numerical analysis of concrete material properties at high strain rate under direct tension”, *J. Impact Eng.*, **39**(1), 51-62.

Hillerborg, A., Modeer, M. and Petersson, P.E. (1976), “Analysis of crack formation and crack growth in concrete by means of fracture mechanics and finite elements”, *Cement Concrete Res.*, **6**(6), 773-781.

Holmquist, T.J., Johnson, G.R. and Cook, W.H. (1993), “A computational constitutive model for concrete subjected to

large strains, high strain rates, and high pressure", *Proceedings of the 14th International Symposium on Ballistics*, Quebec, Canada.
Kwak, H.G. and Filippou, F.C. (1990), *Finite Element Analysis of Reinforced Concrete Structures under Monotonic Load*, Research Report of Department of Civil Engineering, U.C. Berkeley, U.S.A.
Kwak, H.G. and Gang, H.G. (2015), "An improved criterion to minimize FE mesh-dependency in concrete structures under high strain rate conditions", *J. Impact Eng*., **86**, 84-95.
Kwak, H.G. and Song, J.Y. (2002), "Cracking analysis of RC members using polynomial strain distribution function", *Eng. Struct*., **24**(4), 455-468.
Li, Q.M. and Meng, H. (2003), "About the dynamic strength enhancement of concrete-like materials in a split Hopkinson pressure bar test", *J. Sol. Struct*., **40**(2), 343-360.
Lim, S.J., Ahn, K.H., Huh, H., Kim, S.B. and Kim, H.W. (2013), "Fracture evaluation of metallic materials at intermediate strain rates", *Mater. Character*., 171-179.
Lin, X., Zhang, Y.X. and Hazell, P.J. (2014), "Modelling the response of reinforced concrete panels under blast loading", *Mater. Des*., **56**, 620-628.
Lin, Y.C., Chen, M.S. and Zhong, J. (2008), "Effect of temperature and strain rate on the compressive deformation behavior of 42CrMo steel", *J. Mater. Process. Technol*., **205**(1), 308-315.
Lu, Y.B. and Li, Q.M. (2011), "About the dynamic uniaxial tensile strength of concrete-like materials", *J. Impact Eng*., **38**(4), 171-181.
Magnusson, J. and Hallgren, M. (2003), *High Performance Concrete Beams Subjected to Shock Waves from Air Blast*, Swedish Defence Research Agency, Sweden.
Murray, Y.D. (2007), *Users Manual for LS-DYNA Concrete Material Model 159*, Federal Highway Administration, Washington, U.S.A.
Peirs, J., Verleysen, P., Van Paepegem, W. and Degrieck, J. (2011), "Determining the stress-strain behaviour at large strains from high strain rate tensile and shear experiments", *J. Impact Eng*., **38**(5), 406-415.
Rabczuk, T. and Eibl, J. (2006), "Modelling dynamic failure of concrete with meshfree methods", *J. Impact Eng*., **32**(11), 1878-1897.
Roesler, J., Paulino, G.H., Park, K. and Gaedicke, C. (2007), "Concrete fracture prediction using bilinear softening", *Cement Concrete Compos*., **29**(4), 300-312.
Schwer, L.E. and Malvar, LJ. (2005), *Simplified Concrete Modeling with* MAT_CONCRETE_DAMAGE_REL3*, LS-DYNA Anwenderforum, Bamberg, Germany.
Scott, B.D., Park, R. and Priestley, M.J.N. (1982), "Stress-strain behavior of concrete confined by overlapping hoops at low and high strain rates", *ACI J*., **79**(1), 13-27.
Seabold, R.H. (1970), *Dynamic Shear Strength of Reinforced Concrete Beams-Part 3*, U.S. Naval Civil Engineering Laboratory, U.S.A.
Shkolnik, I.E. (2008), "Influence of high strain rates on stress-strain relationship, strength and elastic modulus of concrete", *Cement Concrete Compos*., **30**(10), 1000-1012.
Sluys, L.J. and De Borst, R. (1992), "Computational modelling of impact tests on steel fibre reinforced concrete beams", *Comput. Mech. Compos. Mater*., Heron, **37**(4), 3-15.
Sung, J.H., Kim, J.H. and Wagoner, R.H. (2010), "A plastic constitutive equation incorporating strain, strain-rate, and temperature", *J. Plastic*., **26**(12), 1746-1771.
Tu, Z. and Lu, Y. (2010), "Modifications of RHT material model for improved numerical simulation of dynamic response of concrete", *J. Impact Eng*., **37**(10), 1072-1082.
Unosson, M. and Nilsson, L. (2006), "Projectile penetration and perforation of high performance concrete: Experimental results and macroscopic modelling", *J. Impact Eng*., **32**(7), 1068-1085.
Van Vliet, M.R. and Van Mier, J.G. (2000), "Experimental investigation of size effect in concrete and sandstone under uniaxial tension", *Eng. Fract. Mech*., **65**(2), 165-188.
Vonk, R.A. (1993), *A Micromechanical Investigation of Softening of Concrete Loaded in Compression*, Stevin-Laboratory of the Faculty of Civil Engineering, U.S.A.
Wittmann, F.H., Rokugo, K., Bruhwiler, E., Mihashi, H. and Simonin P. (1988), "Fracture energy and strain softening of concrete as determined by means of compact tension specimens", *Mater. Struct*., **21**(1), 21-32.
Yan, D. and Lin, G. (2007), "Dynamic behaviour of concrete in biaxial compression", *Mag. Concrete Res*., **59**(1), 45-52.
Zhang, X.X., Ruiz, G., Yu, R.C. and Tarifa, M. (2009), "Fracture behaviour of high-strength concrete at a wide range of loading rates", *J. Impact Eng*., **36**(10), 1204-1209.

CC